Epitaxial Ferroelectric Heterostructures with Nanocolumn-Enhanced Dynamic Properties

Marina Tyunina, Lide Yao, Maxim Plekh, Juhani Levoska, and Sebastiaan van Dijken**

The possibility to tailor ferroelectricity by controlling epitaxial strain in thin films and heterostructures of complex metal oxides is well established. Here it is demonstrated that apart from this mechanism, 3D film growth during heteroepitaxy can be used to favor specific domain configurations that lead to step-like polarization switching and a giant nonlinear dielectric response in sub-switching ac electric fields. A combination of cube-on-cube epitaxial growth and the formation of columnar structures during pulsed laser deposition of $Pb_{0.5}Sr_{0.5}TiO_3$ films on $La_{0.5}Sr_{0.5}CoO_3$ bottom electrode layers and MgO (001) substrates stabilizes ferroelectric nanodomains with enhanced dynamic properties. In the $Pb_{0.5}Sr_{0.5}TiO_3$ films, *a*- and *c*-oriented epitaxial columns grow from the bottom to the top of the film leading to random polydomain architectures with strong associations between the ferroelectric domains and the nanocolumns. Polarization switching in the two domain populations is initiated at distinctive fields due to domain wall pinning on column boundaries. Moreover, piezoelectric coupling between ferroelectric domains leads to strong interdomain elastic interactions, which result in an enhanced Rayleigh-type dielectric nonlinearity. The growth of epitaxial films with 3D columnar structures opens up new routes towards the engineering of enhanced ferroelectric and electromechanical functions in a broad class of complex oxide materials.

1. Introduction

Complex metal oxides, especially perovskite-structure oxides, exhibit a rich variety of electronic states (from insulating to superconducting) and ferroic ordering phenomena (ferroelectric, ferromagnetic, multiferroic). The mutual chemical and structural compatibility of these oxides allows for the fabrication of multilayer heterostructures with novel and controllable functions. Completely new electronic devices using such oxide heterostructures are now emerging, establishing a rapidly growing field of research and development. Their main application area is foreseen in future morphic computational systems.[1–3] Epitaxial films of perovskite-type ferroelectrics (FEs), whose polarization and/or resistivity can be modified electrically in a non-volatile manner, may be relevant for such systems. In a broader sense, the applications of FE films are connected with the diversification of electronic devices and systems, where FE epitaxial single-crystal films may have superior performance compared to nanocrystalline films (e.g., higher permittivity) or may bring novel functions (e.g., strong magnetoelectric effect). Here we demonstrate epitaxial FE films which possess enhanced dynamic properties including step-like polarization switching and strong dielectric nonlinearity.

Compared to bulk samples, the plethora of properties of perovskite-type oxides is spectacularly enriched in epitaxial films of these materials.[4,5] In particular, the phase diagrams and properties of heteroepitaxial films can be considerably altered by variation of the misfit strain *s*.[4,6,7] The misfit strain arises from a mismatch between the lattice parameter a_s of the substrate and the in-plane lattice parameter a_f of the film, and it is usually defined as $s = (a_f/a_s - 1)$. In heteroepitaxial films of FEs, the influence of biaxial in-plane misfit strain on FE behavior is mainly realized via indirect coupling between *s* and the magnitude of ferroelectric polarization.[6] Besides, the division of FEs into domains also depends strongly on *s*.[8–11] Because FE domains and domain walls are responsible for key properties of FEs such as total polarization and polarization switching, the ability to control FE domain configurations in heteroepitaxial films is of great practical importance. Moreover, it is well established that domain wall motion plays a dominant role in the dynamic dielectric and piezoelectric response of FEs.[11–14] In particular, it is widely accepted that the motion of non-180° domain walls increases the dielectric permittivity and piezoelectric coefficient in sub-switching ac electric fields (E_{AC}). In this field range, the real part ε of the dielectric permittivity is approximated by the Rayleigh law $\varepsilon(E_{AC}) = \varepsilon(0) + \alpha E_{AC}$, where α indicates the irreversible Rayleigh coefficient. The dynamic dielectric nonlinearity is often characterized by the ratio $\alpha/\varepsilon(0)$.[14] In epitaxial single-domain FE films, domain wall motion is absent and the nonlinearity is zero: $\alpha/\varepsilon(0) = 0$. In epitaxial polydomain FE films with striped *a*-*c* domain patterns, the motion of the non-180°

Dr. M. Tyunina, M. Plekh, J. Levoska
Microelectronics and Materials Physics Laboratories
University of Oulu
P. O. Box 4500, FI-90014 Oulun Yliopisto, Finland
E-mail: marinat@ee.oulu.fi
Dr. L. D. Yao, Prof. S. van Dijken
NanoSpin, Department of Applied Physics
Aalto University School of Science
P. O. Box 15100, FI-00076 Aalto, Finland
E-mail: sebastiaan.van.dijken@aalto.fi

DOI: 10.1002/adfm.201201528

domain walls is strongly limited by substrate clamping and inter-domain pinning. As a result, the nonlinearity is small. Mobile polydomain architectures have been devised to enhance the nonlinear dielectric and piezoelectric response,[10] but the need for epitaxial FE films with a specific composition or orientation makes this approach less versatile. In polycrystalline ceramics-type FE films of submicron thickness, small grain sizes, substrate clamping, and domain pinning lead to relatively small nonlinearities of $\alpha/\varepsilon(0) \sim 10^{-7}$ mV^{-1}.[12–14] Obtaining FE films with improved non-linear dynamic properties is a challenging task.

Here, we present epitaxial FE heterostructures in which the FE domain configuration and the dynamic dielectric response are controlled by the formation of epitaxial columns. As a FE material we have selected $Pb_{0.5}Sr_{0.5}TiO_3$ (PSTO). In its bulk ceramic form, PSTO possesses rather poor ferroelectric, piezoelectric, or nonlinear properties compared to those in Pb(Zr,Ti)O_3 or $PbMg_{1/3}Nb_{2/3}O_3$–$PbTiO_3$.[12,15] However, ease of formation of the pure perovskite phase and absence of low-temperature structural phase transitions make PSTO especially attractive from the point of view of thin-film technology. The heterostructures consist of pulsed-laser deposited epitaxial perovskite PSTO films on top of relatively thick (100–200 nm) $La_{0.5}Sr_{0.5}CoO_3$ (LSCO) bottom electrode layers and MgO (001) single crystal substrates (Supporting Information S1). The large misfit between the lattice parameters of LSCO and MgO (s = –9.0%) promotes 3D film growth without the destruction of epitaxy, and this growth mode continues in the PSTO film. Moreover, the epitaxial relationships are sustained across boundaries of the formed epitaxial columns, which is an important distinction from grain or columnar boundaries in polycrystalline and textured films. Strong correlations between the epitaxial columns and FE domains are evidenced by a combination of X-ray diffraction analysis, high-resolution transmission electron microscopy, and piezoresponse force microscopy. The heterostructures with epitaxial columns exhibit an unusual FE response including step-like polarization switching and a strong sub-switching dielectric nonlinearity with a ratio $\alpha/\varepsilon(0)$ that is considerably larger than those observed for polycrystalline and textured films.

2. Results and Discussion

2.1. Structural Properties

Epitaxial growth and column formation in PSTO/LSCO/MgO heterostructures are demonstrated by X-ray diffraction (XRD) and high-resolution transmission electron microscopy (HR-TEM). XRD analysis (Supporting Information S2) shows that both the LSCO and perovskite PSTO layers are highly oriented with (00l) planes parallel to the (001) surface of the MgO substrate (**Figure 1**). The crystal structure of LSCO on MgO can be interpreted as tetragonal, with measured in-plane and out-of-plane lattice parameters of $a_{LSCO} \approx 3.864$ Å and $c_{LSCO} \approx 3.805$ Å. Considering the lattice parameter of the bulk pseudocubic LSCO target (a_{bulk} = 3.835 Å),[16,17] the average residual in-plane tensile strain in the LSCO film is given by $(a_{bulk}/a_{LSCO} - 1) \approx -0.8\%$, which is much smaller than the LSCO/MgO lattice mismatch of –9%. Most of the misfit strain is probably released by the formation of a regular network of misfit dislocations at the LSCO/MgO interface, whose period Λ is estimated by $\Lambda \approx 0.5(a_{LSCO})^2/(a_{MgO}-a_{LSCO})$. Using the bulk lattice parameters of LSCO and MgO, this gives $\Lambda \approx 21$ Å. For such high-density dislocation networks, a transition from layer-by-layer to 3D film growth commonly occurs.[18] The suggested 3D growth mode does not disturb the epitaxy. The LSCO layer grows epitaxially on the MgO substrate and the cube-on-cube type epitaxial relationship is given by LSCO [100](001) || MgO [100](001).

The crystal structure of the PSTO films is also tetragonal. From the PSTO reflections, the two out-of-plane lattice parameters are determined as $c_1 \approx 3.923$ Å and $c_2 \approx 3.965$ Å. The corresponding in-plane lattice parameters are $a_1 \approx 3.963$ Å and $a_2 \approx 3.924$ Å, respectively. These parameters agree well with the room-temperature tetragonal crystal structure and lattice parameters of bulk PSTO,[15] indicating relaxation of the PSTO/LSCO misfit strain (1.6% or 2.6% depending on domain type) via 3D growth. The PSTO films contain *c*-oriented domains (elongated lattice parameter perpendicular to the film plane) and *a*-oriented domains (elongated lattice parameter in the film plane). For both domain types, the in-plane epitaxial relationship is given by PSTO [100](001) || LSCO [100](001) || MgO [100](001). The volume fractions of *a*- and *c*-domains estimated from the integrated intensity of the PSTO (004) peaks are 0–35% and 100–65%, depending on the PSTO deposition rate. The out-of-plane coherence length is found to be approximately equal to the film thickness implying that the domains grow vertically from the bottom to the top of the PSTO films, in contrast to the striped *a*/*c* FE domain configurations that are often observed in layer-by-layer grown FE films.[8,9]

Cross-sectional TEM images of the heterostructures clearly reveal the presence of column-like features in both the LSCO and PSTO layers (**Figure 2**). In the out-of-plane direction, the

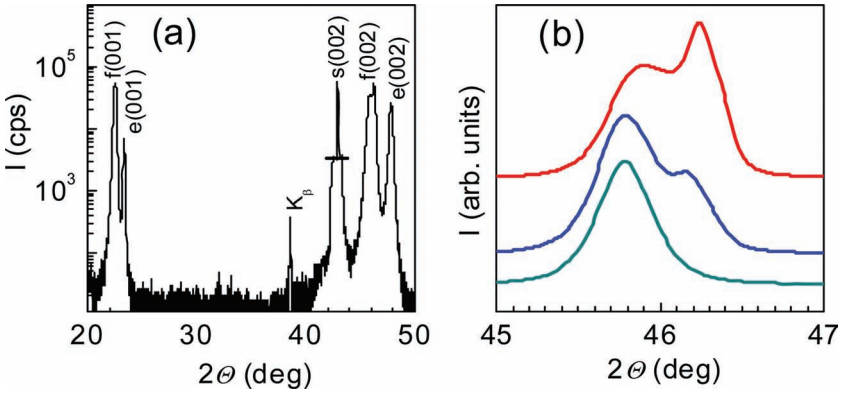

Figure 1. a) θ–2θ X-ray diffraction pattern of the PSTO/LSCO/MgO(001) heterostructure. The intensity of the substrate (002) reflection is reduced by filtering (as indicated by the straight line). The reflections from the PSTO film, the LSCO electrode, and the MgO substrate are marked by f, e, and s, correspondingly. b) θ–2θ scans of the PSTO (002) reflections indicating different volume fractions of *a* and *c*- domains for three different 260 nm thick PSTO films. The volume fraction of *a*-domains increases from the bottom to the top curve.

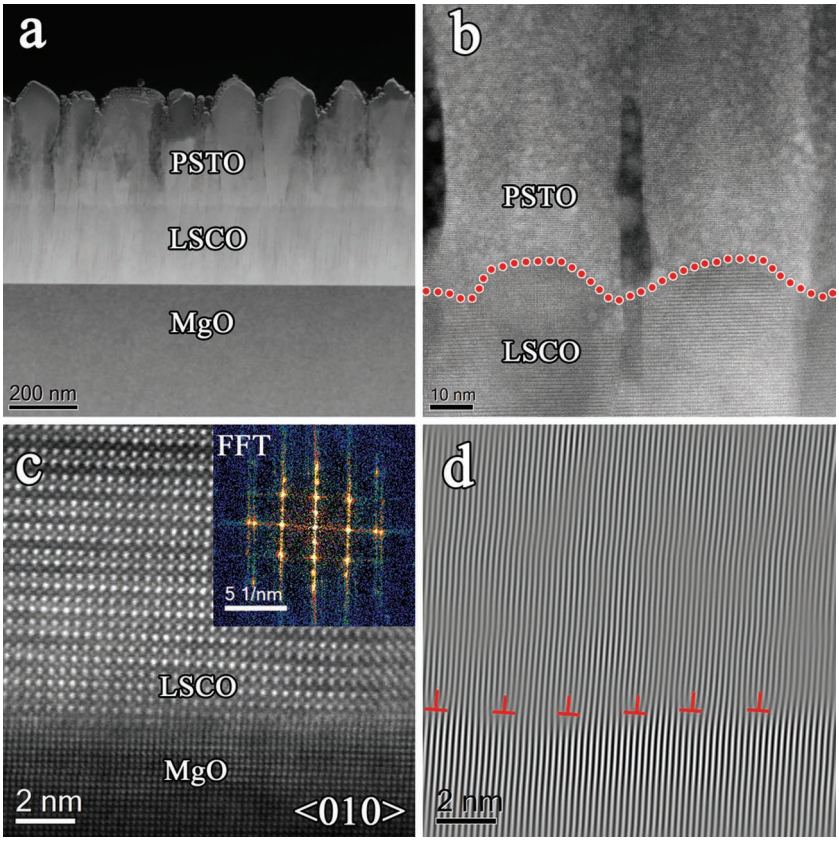

Figure 2. a) Low magnification cross-sectional Z-contrast image of a PSTO/LSCO/MgO heterostructures. b) Z-contrast image of the PSTO/LSCO interface. c) High-resolution Z-contrast image of the LSCO/MgO interface along the <010> zone axis. The inset shows the FFT pattern. d) Selected (200) FFT filter image corresponding to (c).

boundaries between the columns are not strictly normal to the substrate surface and they are not well resolved throughout the whole thickness of the LSCO/PSTO stack. In the PSTO film, the in-plane widths of the columns are about 50–100 nm, whereas the average width is smaller in LSCO. Some of the boundaries that originate in the LSCO bottom layer, continue in the PSTO film (Figure 2a,b). The LSCO and PSTO surface roughness correlates with these features. The detected microstructure agrees with 3D film growth, whereby the 3D nanostructures manifest themselves as columns in the as-grown heterostructures. High-resolution Z-contrast imaging and local fast Fourier transform (FFT) analysis (Figure 2c) evidence epitaxial growth of LSCO on MgO, in agreement with XRD analysis. The epitaxial relationship is confirmed as LSCO [100](001) || MgO [100](001). The selected (200) FFT filter image (Figure 2d) shows that a network of misfit dislocations forms in the LSCO layer near the MgO surface. The measured network period Λ is about 20 Å, which is in excellent agreement with the period $\Lambda \approx 21$ Å as estimated from the XRD results. The TEM measurements clearly reveal that the epitaxial relationship is sustained across the boundaries between columns. This is in contrast to grain or columnar boundaries in polycrystalline or textured films. To emphasize this difference and the direct connection between the formation of structural boundaries and the 3D epitaxial growth mode, the column-like features are referred to as "epitaxial columns" in this paper. In addition to epitaxial columns, the LSCO film also contains a superstructure with every second CoO_2 layer displaying dark contrast (Figure 2c). In the corresponding FFT pattern, the reflections from the superlattice are observed between primitive structural spots. This effect has also been measured on strained epitaxial LSCO films deposited by magnetron sputtering.[19] It has been suggested in ref. [19] that the superstructure contrast may be related to the formation of an ordered structure of oxygen vacancies. A similar type of ordering has been recently observed in epitaxial manganite films.[20]

TEM analysis also confirms epitaxial growth of the PSTO films (Figure 2b and **Figure 3**a). The epitaxial relationship is PSTO [100](001) || LSCO [100](001), consistent with XRD data. In the PSTO film, an epitaxial column boundary can be distinguished at about 20 nm above the LSCO/PSTO interface (Figure 3a). In the selected region around this feature (as marked in Figure 3a), a more detailed analysis of atomic positions is performed. As seen in Figure 3b, two edge dislocations are detected below the boundary (marked by "T"symbols). One is located within the LSCO film just below the PSTO-LSCO interface, while the other appears in the PSTO film above the interface, at about 10 nm from the first dislocation. Both dislocations are characterized by the same Burger's vector, $\mathbf{b} = a$ [100]. In the PSTO film, a stacking fault is found along the (100) plane above the dislocations. It represents a boundary of two Ti-O layers, separating two regions marked by I and II in Figure 3c. In both regions,the out-of-plane lattice parameter is slightly larger than the in-plane parameter and thus both regions belong to epitaxial *c*-domains. The obtained ratio $c/a \approx 1.01$ is consistent with XRD measurements. As can be seen in the corresponding schematic of Figure 3d, the perovskite [TiO_2] and [(Pb/Sr)O] atomic planes in region I are displaced in the out-of-plane direction by half a unit cell with respect to the planes in region II. As a result, the boundary consists of two [TiO_2] planes, which suggests that the 3D columns that form during PSTO film growth are TiO-terminated. The observed Ti-rich boundaries resemble those in epitaxial $BaTiO_3$ films.[21] In an attempt to get a better insight in the nature of other structural boundaries, the elemental composition of PSTO at different column boundaries was inspected using energy-dispersive X-ray spectroscopy (Supporting Information S3). A clear difference between the PSTO stoichiometry in the center of epitaxial columns and at their boundaries was not revealed.

2.2. Ferroelectric Domains

In the PSTO/LSCO/MgO heterostructures, self-consistent results of XRD and TEM analyses evidence epitaxial cube-on-cube

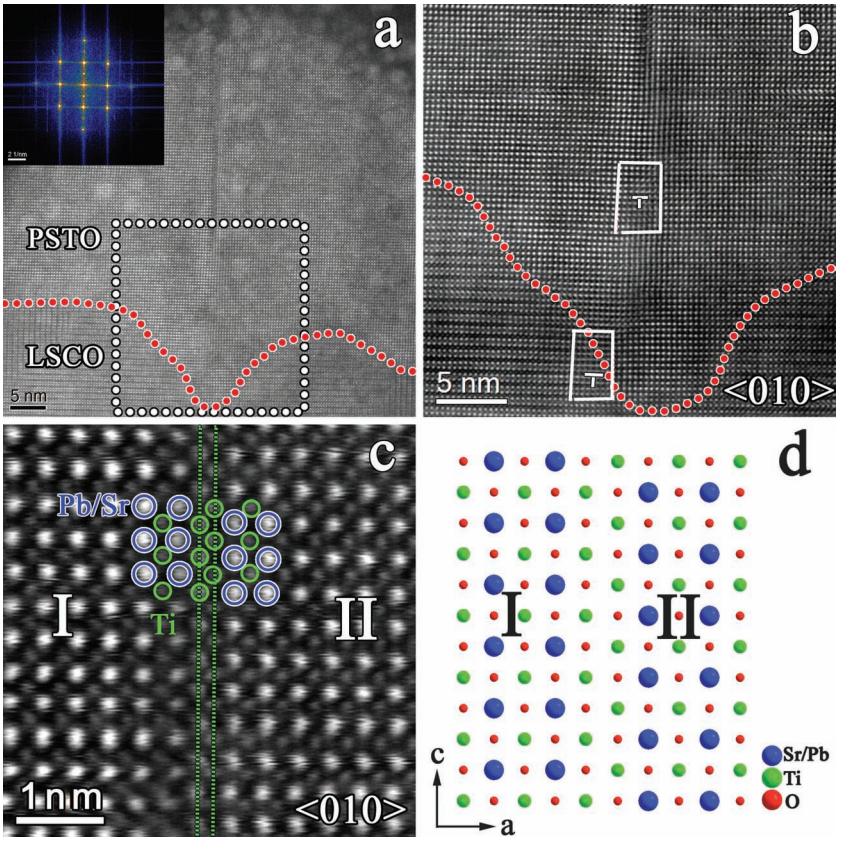

Figure 3. a) Z-contrast image of the PSTO/LSCO interface including structural defects. The inset shows the corresponding FFT pattern. b) High magnification Z-contrast image from the selected area in (a) exhibiting edge dislocations along the <010> zone axis. The Burger circuits are denoted by white outlines. c) High-resolution Z-contrast image of the PSTO film with a typical stacking fault column boundary. d) Structural schematic of the stacking fault in (c).

growth in combination with the formation of epitaxial columns. In the tetragonal PSTO films, *a*- and *c*-oriented structural columns coexist. Their relation to the FE domain configuration is inspected by piezoresponse force microscopy (PFM) using a Pt top electrode (Supporting Information S4). The PFM response in the out-of-plane and in-plane directions indicates the coexistence of two polarization directions, in agreement with the presence of structural *a*- and *c*-domains. The PFM images reveal randomly arranged domains with lateral dimensions of about 100–500 nm. The FE domains embrace one to several structural features with a width of 50–100 nm and the FE domain boundaries are abrupt and facetted (**Figure 4**). Neighboring epitaxial columns in the PSTO film with the same crystal structure, epitaxial relationship, lattice parameters, and polarization direction, constitute one larger FE domain. Many of the column boundaries also serve as boundaries between FE domains with different directions of polarization. More importantly, all FE domain walls are associated with epitaxial column boundaries. As illustrated in **Figure 5**, this domain configuration has no analogy in other FE films or bulk FE materials. In polycrystalline or textured films (Figure 5a,b), the grains contain one or several domains and the crystal lattice is discontinuous across grain boundaries.[13,22] In our PSTO films (Figure 5e,f), on the other hand, the epitaxial columns only consist of one FE domain and the epitaxial relationships are sustained across column boundaries. Finally, in uniform epitaxial films the domain patterns are not limited by column or grain boundaries and elongated stripe domains form (Figure 5c,d). We note that the size of FE domains in the PSTO films is artificially reduced by the presence of structural epitaxial columns as compared to the elongated stripe domains in uniform epitaxial films (Figure 5g,h). Under an applied electric field, the high density of column boundaries leads to non-uniform FE polarization switching and strong enhancement of the nonlinear dielectric response as demonstrated in the next two sections.

2.3. Polarization Switching

In the Pt/PSTO/LSCO/MgO capacitor heterostructures, switching of the FE polarization is indicated by switching current and polarization loops (**Figure 6**). The electric field in these measurements is applied perpendicular to the PSTO film. In some heterostructures, the loops are shifted along the field axis. Such an offset is commonly ascribed to a difference between the work functions of the top and bottom electrode materials, which can be influenced by polarization.[23–25] The (*P*–*E*) loops are symmetric with respect to the maximum values of polarization in opposite directions, i.e., $P_{max} \approx -P_{max}$. The current-field loops exhibit current peaks which are relatively broad compared to those typically observed in single-domain epitaxial films.[26] Different switching fields of separate domains leading to a distribution of switching fields instead of a single field value can explain such behavior. The maximum current that is measured at the switching field, E_{SW}, reflects switching of the largest portion of domains in the PSTO film. The switching field E_{SW} and the maximum polarization P_{max} depend on

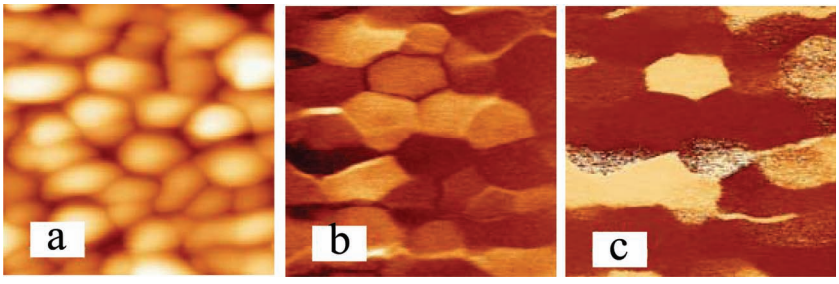

Figure 4. AFM and PFM images of a PSTO/LSCO/MgO heterostructure. Thickness of the PSTO film is 130 nm, and fraction of the *a*–domains is ≥30%. a) Topography, b) amplitude and c) phase of the in-plane PFM response. The scan size is 0.4 μm × 0.4 μm.

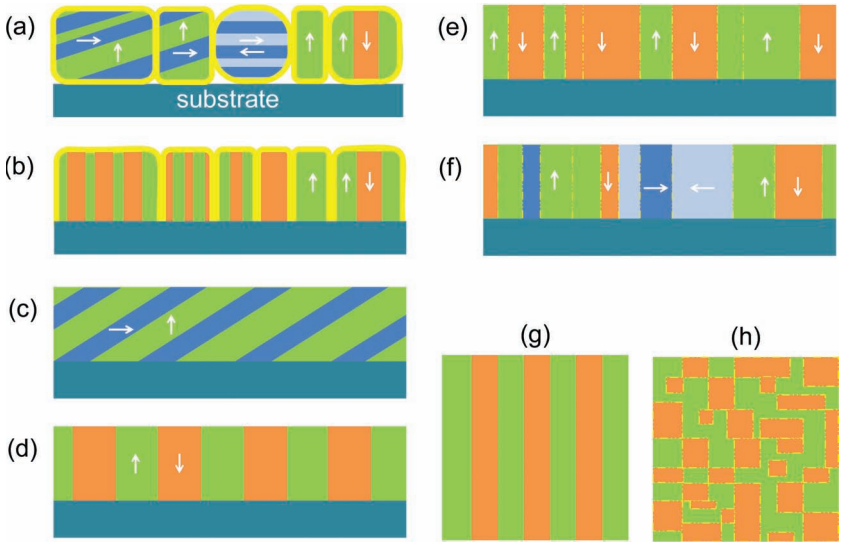

Figure 5. Schematic polydomain architectures in FE films. a–f) Cross-section of a) a polycrystalline film with grain boundaries, b) a textured (001) oriented film with 180° domains and grain boundaries, c) a uniform epitaxial film with non-180° stripe domains, d) a uniform epitaxial film with 180° stripe domains, e) an epitaxial film with 180° domains associated with structural nanocolumns, and f) an epitaxial film with 180° and non-180° domains associated with structural nanocolumns. The arrows indicate the direction of polarization inside the domains. g,h) Schematic top view of two films with 180° domains: g) in a uniform epitaxial film shown in (d) and h) in an epitaxial film with nanocolumns shown in (e).

the maximum applied field E_{max}. These dependencies are used to compare polarization switching in the PSTO films of similar thickness, but with different *a*- and *c*-domain populations (**Figure 7**). For films that contain mainly *c*-domains, the switching field weakly increases with increasing E_{max} (Figure 7a). This suggests a narrow distribution of local switching fields of FE nanodomains. In this case, the fraction of switched domains and the maximum polarization grow with increasing E_{max} (Figure 7b). However, for films containing both *a*- and *c*-domains, the switching field strongly rises at $E_{max} \approx 40$ MVm^{-1} (Figure 7a). This is accompanied by a corresponding rise in P_{max} (Figure 7b). Such a step-like switching behavior can be explained by the coexistence of two FE domain populations with distinctive switching fields. Moreover, it suggests that polarization switching in the *c*-domains has little effect on switching in the *a*-domains and vice versa. This can be understood by comparing the schematic domain configurations of Figure 5c,f. In the PSTO films, the displacement of non-180° domain walls, which is typical for switching in epitaxial films with a striped *a*/*c* FE domain pattern,[9] is prohibited by the presence of epitaxial column boundaries. An alternative switching mechanism that decouples polarization switching in *a*- and *c*-domains may involve rotation of polarization in *a*-domains, nucleation at column boundaries, and other switching effects. The observed step-like switching phenomenon could potentially be interesting for multistate memory devices and deserves further investigation.

2.4. Nonlinear Dielectric Response

It is widely accepted that the Rayleigh-type dynamic dielectric nonlinearity in FEs is mainly determined by the motion of FE domain walls. In our epitaxial PSTO films with epitaxial columns, the domain walls are clamped by column boundaries and, hence, the motion of domain walls is strongly limited if not impossible. Nevertheless, the dielectric permittivity of the PSTO heterostructures increases with increasing amplitude E_{AC} and follows the Rayleigh law $\varepsilon(E_{AC}) = \varepsilon(0) + \alpha E_{AC}$. This is illustrated in **Figure 8**a where the normalized nonlinear dielectric permittivity (or nonlinearity for brevity) $\Delta\varepsilon/\varepsilon(0) = (\varepsilon(E_{AC}) - \varepsilon(0))/\varepsilon(0)$ is plotted versus E_{AC}. The nonlinearity starts to deviate from the Rayleigh-type behavior at $E_{AC} > 4 \times 10^6$ Vm^{-1}, which is similar to observations in FE ceramics and normally indicates the onset of modification of domain pattern or partial polarization switching. In the sub-switching regime, the nonlinearity dependence on frequency is mainly determined by capacitor design.[27] Here, the nonlinearity at 1 kHz of PSTO capacitor heterostructures with a 260 nm thick PSTO film is compared with that of capacitors with FE films of similar thickness, namely polycrystalline PSTO (poly-PSTO) grown on $SrRuO_3$/MgO(001),[28] polycrystalline $PbTiO_3$ (PTO) and textured (001) oriented $PbZr_{0.53}Ti_{0.47}O_3$ (PZT).[13,14] The nonlinearity is remarkably enhanced in the PSTO capacitors with epitaxial columns (Figure 8a). For PSTO with epitaxial columns, the slope $\alpha/\varepsilon(0)$ is about 3×10^{-7} mV^{-1}, which considerably exceeds the values of 0.96×10^{-7} mV^{-1} for PTO, and $\approx 0.6 \times 10^{-7}$ mV^{-1} for PZT and poly-PSTO. Our experiments do not indicate a clear correlation between $\alpha/\varepsilon(0)$ and the volume fraction of *a*- and *c*-domains in the PSTO films. On the other hand, a decrease of the PSTO film thickness to 130 nm is found to reduce $\alpha/\varepsilon(0)$ to $(1.5–1.8) \times 10^{-7}$ mV^{-1}, which is most likely due to the presence of near-electrode interfacial capacitance.[27]

The large nonlinearity of PSTO heterostructures is connected with the FE state. Indeed, as can be seen in Figure 8b, the nonlinearity is only observed at temperatures below the temperature T_m of the dielectric maximum, i.e., when the PSTO is FE, while the nonlinearity is absent in the high-temperature paraelectric state (above T_m). However, since the FE domain walls are clamped by the epitaxial column boundaries (Figure 5e,f), the nonlinearity cannot originate from the commonly accepted motion of FE domain walls. It is worth noting that recent studies on FE ceramics using time-resolved high-energy XRD analysis have shown that electrically induced lattice strain can account for approximately 40% of the Rayleigh-like piezoelectric nonlinearity.[29] The lattice strain in these FE ceramics originates from elastic intergranular interactions. In such polycrystalline randomly oriented FEs (Figure 5a), the differently oriented grains exhibit distinctive degrees of non-180° domain wall motion. Grains with efficient non-180° domain wall motion impose a strain in the matrix, and other less favorably oriented grains elastically accommodate this strain.[29] The suggested scenario is not directly transferrable to our PSTO films without mobile ferroelastic domain walls. In epitaxial films with epitaxial columns, however, the adjacent domains can elastically interact through piezoelectric coupling. For instance, application

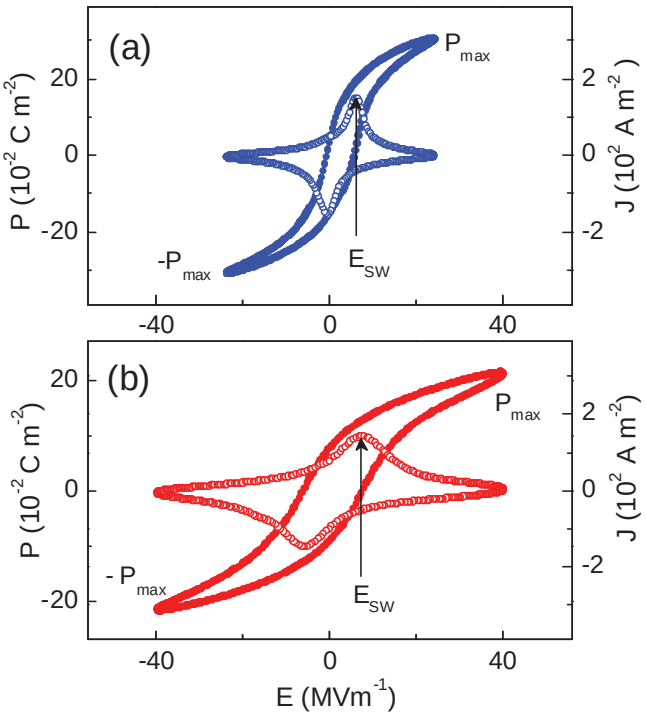

Figure 6. Polarization P (solid symbols) and current density J (open symbols) as a function of applied electric field E measured at room temperature in Pt/PSTO/LSCO/MgO capacitor heterostructures with a PSTO film thickness of 260 nm. The volume fraction of *a*-domains in the PSTO film is less than 5% in (a) and about 35% in (b). The arrows illustrate how the switching field E_{SW} is determined from these measurements.

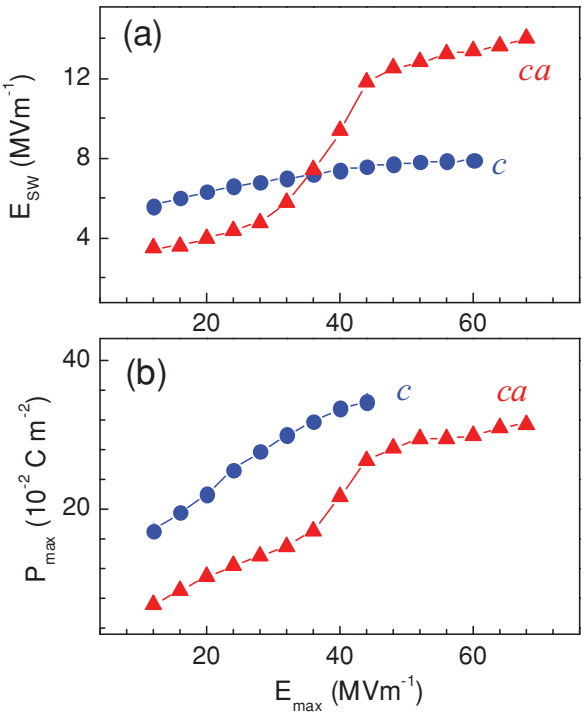

Figure 7. Switching field E_{SW} (a) and maximum polarization P_{max} (b) as a function of maximum applied field E_{max} as measured on Pt/PSTO/LSCO/MgO capacitor heterostructures. The volume fraction of *a*-domains in the 260 nm thick PSTO film is less than 5% (blue circles marked by *c*) and about 35% (red triangles marked by *ca*).

of an electric field in the out-of-plane direction would cause converse piezoelectric tensile strain in "up" *c*-domains, compressive strain in "down" *c*-domains, and minor strain in *a*-domains. Due to the mechanical compatibility of the domains and the continuity of epitaxy across column boundaries, the dissimilarity in piezoelectric strain acts as a source of inhomogeneous internal film stress, which can modify spontaneous strain, polarization, and dielectric permittivity.[30,31]

As seen from Figure 5d,e, the FE domain configuration of films with epitaxial columns resembles that of epitaxial films with 180° domains. It has been emphasized in ref. [[30]] that such 180° FE domains are elastically identical without electric field but start behaving as elastic domains under an external electric field. Indeed, under an electric field, the converse piezoelectric strains in 180° domains have opposite signs: one domain elongates while the other shrinks longitudinally. The difference in piezoelectric strain is a source of internal stresses and interdomain clamping. This effect modifies the dielectric and piezoelectric responses of thin films with 180° domains. The thermodynamic analysis presented in ref. [30] has given an effective dielectric permittivity which is directly proportional to the applied electric field. Remarkably, such dependence is formally equivalent to the Rayleigh law. Since our films with epitaxial columns contain mechanically compatible 180° domains and possess the continuity of epitaxy across domain boundaries, the results of this analysis can be applied to explain the strong dynamic nonlinearity in our films. The observed dependence of the dielectric permittivity on field amplitude in the PSTO films is in qualitative agreement with the theoretical analysis.[30]

Compared to an epitaxial film composed of 180° domains (Figure 5d), films with epitaxial columns (Figure 5e) possess a more stable domain configuration. Moreover, as the FE domain walls are effectively pinned onto the nanocolumn boundaries, the FE domains in our films are less sensitive to surface boundary conditions. Finally, epitaxial films with columnar nanostructures possess a higher density of domain boundaries compared to films with striped 180° domains. These factors are favorable for the design of enhanced nonlinear dynamic responses. Epitaxially controlled nonlinearities can thus be employed to develop advanced piezoelectric and dielectric heterostructures.

Finally, we note that nanocolumn-enhanced dynamic properties are not necessarily restricted to epitaxial systems with large lattice mismatch. While in our experiments the formation of PSTO columns is promoted by 3D film growth of LSCO on MgO ($s = -9.0\%$), large misfit strains are not the only necessary reason for this growth mode. Similar growth modes are also possible for a small film-substrate lattice mismatch or even its complete absence.[18] For a given film-substrate combination, the growth mode depends sensitively on the surface free energy of both materials, the film deposition rate, and the growth temperature and therefore it can be adjusted by selecting the appropriate surface termination and growth conditions. Engineering of FE properties by controlling the growth mode may further broaden the spectrum of functions in complex oxide heterostructures.

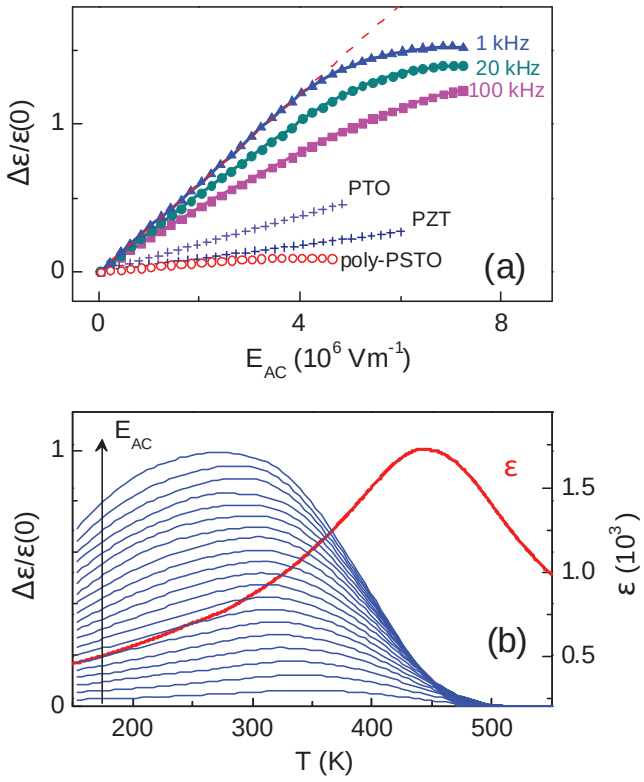

Figure 8. Dielectric response of a Pt/PSTO/LSCO/MgO capacitor heterostructure with a 260 nm thick PSTO film containing an *a*-domain fraction of about 35%. a) Nonlinearity $\Delta\varepsilon/\varepsilon(0)$ as a function of amplitude E_{AC} of ac driving field at a temperature of $T = 303$ K and different frequencies. The dashed line is a linear fit to the data for $f = 1$ kHz. The room temperature behavior of capacitors with 260 nm thick films of polycrystalline $Pb_{0.5}Sr_{0.5}TiO_3$ (poly-PSTO), polycrystalline $PbTiO_3$ (PTO), and textured (001) oriented $PbZr_{0.53}Ti_{0.47}O_3$ (PZT) is shown for comparison.[13,14,28] b) Nonlinearity $\Delta\varepsilon/\varepsilon(0)$ as a function of temperature T at different $E_{AC} = (0.02–4) \times 10^6$ Vm^{-1} and a frequency of 20 kHz. The arrow indicates the direction of increasing E_{AC}. The dielectric permittivity ε measured at $E_{AC} = 2 \times 10^4$ Vm^{-1} and 20 kHz is also presented (solid red line).

3. Conclusions

In this paper, we reported on anomalous FE polarization switching and dielectric nonlinearities in epitaxial PSTO/LSCO/MgO heterostructures. Self-consistent results from XRD, TEM, and AFM/PFM measurements indicate a strong link between the formation of epitaxial columnar structures and FE domain patterns. The FE polarization of each individual column is uniform and, consequently, all FE domain walls coincide with column boundaries. This results in strong domain wall clamping and limited domain wall motion in applied electric fields. Another important feature relates to the column structure. While the tetragonal PSTO films consist of *a*- and *c*-oriented domains, the epitaxial relationships with the LSCO bottom electrode and MgO substrate are sustained across column boundaries. The minimal distortion of the crystalline lattice maximizes the elastic interactions between neighboring domains. Two main FE effects are observed. First, polarization switching in dc electric fields proceeds in a step-like manner indicating distinctive reversal mechanisms in the *a*- and *c*-domains. Second, the application of ac electric fields in the sub-switching regime induces very large dielectric nonlinearities if the PSTO film is in the FE state. Although an exact understanding of the driving mechanisms behind these FE phenomena requires further investigations, our data strongly indicates that the 3D epitaxial growth mode is instrumental for the enhanced dynamic response. Based on these results, we anticipated that the growth of epitaxial films with columnar structures may provide a powerful tool for obtaining new and improved functions in FE and other complex oxide heterostructures.

4. Experimental Section

PSTO/LSCO/MgO heterostructures with 130–260 nm thick PSTO and 100–200 nm thick LSCO films were grown by pulsed laser deposition (Supporting Information S1). For electrical characterization and local imaging of FE domains, Pt top electrodes with a diameter of 0.1–0.7 mm were formed by pulsed laser deposition using shadow masks. The room-temperature crystal structure was studied by X-ray diffraction (XRD) using Cu Kα radiation with a post-monochromator. To study in-plane epitaxy, structural domain configurations, and lattice parameters of the films, the (004) and non-specular (024) reflections were analyzed (Supporting Information S2). The specimen for high-resolution transmission electron microscopy (TEM) analysis were prepared by standard cross-sectional techniques, i.e., face-to-face gluing of the films, subsequent cutting into thin slices, followed by mechanical polishing, dimpling, and Ar ion milling. High-resolution Z-contrast imaging was carried out in a JEOL 2200FS TEM with double C_s correctors, operated at 200 kV. The FE domains were imaged by piezoresponse force microscopy (PFM) using a Veeco Dimension SPM Nanoscope IV and a lock-in technique. Here, an ac probing voltage was applied between the LSCO bottom and the Pt top electrode while a non-conducting tip was in contact with the surface of the Pt film (Supporting Information S4). Electrical characterization of the Pt/PSTO/LSCO/MgO capacitor heterostructures was performed using an HP 4284A LCR meter, a Linkam LTSE350 MultiProbe stage, and a modified Sawyer-Tower circuit.

Supporting Information

Supporting Information is available from the Wiley Online Library or from the author.

Received: June 7, 2012
Published online: August 30, 2012

[1] Z. Yang, C. Ko, S. Ramanathan, *Annu. Rev. Mater. Res.* **2011**, *41*, 337.
[2] S. D. Ha, S. Ramanathan, *J. Appl. Phys.* **2011**, *110*, 071101.
[3] M. Bibes, J. E. Villegas, A. Barthélémy, *Adv. Phys.* **2011**, *60*, 5.
[4] J. M. Rondinelli, N. A. Spaldin, *Adv. Mater.* **2011**, *23*, 3363.
[5] L. W. Martin, Y.-H. Chu, R. Ramesh, *Mater. Sci. Eng. R* **2010**, *68*, 89.
[6] N. A. Pertsev, A. G. Zembilgotov, A. K. Tagantsev. *Phys. Rev. Lett.* **1998**, *80*, 1988.
[7] N. A. Pertsev, *Phys. Rev. B* **2008**, *78*, 212102.
[8] J. S. Speck, A. C. Daykin, A. Seifert, A. E. Romanov, W. Pompe, *J. Appl. Phys.* **1995**, *78*, 1696.
[9] A. Roelofs, N. A. Pertsev, R. Waser, F. Schlaphof, L. M. Eng, C. Ganpule, V. Nagarajan, R. Ramesh, *Appl. Phys. Lett.* **2002**, *80*, 1424.

[10] J. Ouyang, J. Slutsker, I. Levin, D.-M. Kim, C.-B. Eom, R. Ramesh, A. L. Roytburd, *Adv. Funct. Mater.* **2007**, *17*, 2094.
[11] A. K. Tagantsev, L. E. Cross, J. Fousek, *Domains in Ferroic Crystals and Thin Films,* Springer Science+Bussiness Media, New York **2010**, pp. 821.
[12] N. Bassiri-Gharb, I. Fujii, E. Hong, S. Trolier-McKinstry, D. V. Taylor, D. Damjanovic, *J. Electroceram.* **2007**, *19*, 47.
[13] Z. Kighelman, D. Damjanovic, M. Cantoni, N. Setter, *J. Appl. Phys.* **2002**, *91*, 1495.
[14] Y. Bastani, T. Schmitz-Kempen, A. Roelofs, N. Bassiri-Gharb, *J. Appl. Phys.* **2011**, *109*, 014115.
[15] *Landolt-Börnstein, Numerical Data and Functional Relationships in Science and Technology, New Series, Group III, Crystal and Solid State Physics*, (Eds: K. H. Hellwege, A. M. Hellwege), Springer, Berlin **1981**.
[16] J. T. Cheung, P. E. O. Morgan, D. H. Lowndes, X.-Y. Zheng, J. Breen, *Appl. Phys. Lett.* **1993**, *62*, 2045.
[17] As measured in the target used for deposition in the present work.
[18] M. Ohring, *The materials science of thin films*, Academic Press, San Diego **2002**.
[19] D. O. Klenov, W. Donner, B. Foran, S. Stemmer, *Appl. Phys. Lett.* **2003**, *82*, 3427.
[20] J. D. Ferguson, Y. Kim, L. Fitting Kourkoutis, A. Vodnick, A. R. Woll, D. A. Muller, J. D. Brock, *Adv. Mater.* **2011**, *23*, 1226.
[21] J. Q. He, E. Vasco, R. Dittmann, R. H. Wang, *Phys. Rev. B* **2006**, *73*, 125413.
[22] Y. Ivry, D. Chu, J. F. Scott, C. Durkan, *Adv. Funct. Mater.* **2011**, *21*, 1827.
[23] L. Pintilie, I. Vrejoiu, D. Hesse, G. LeRhun, M. Alexe, *Phys. Rev. B* **2007**, *75*, 104103.
[24] L. Pintilie, V. Stancu, L. Trupina, I. Pintilie, *Phys. Rev. B* **2010**, *82*, 085319.
[25] L. Pintilie, I. Vrejoiu, D. Hesse, M. Alexe, *J. Appl. Phys.* **2008**, *104*, 114101.
[26] I. Vrejoiu, G. Le Rhun, L. Pintilie, D. Hesse, M. Alexe, U. Gösele, *Adv. Mater.* **2006**, *18*, 1657.
[27] M. Tyunina, J. Levoska, *Appl. Phys. Lett.* **2006**, *88*, 262904.
[28] M. Tyunina, M. Plekh, M. Antonova, A. Kalvane, *Phys. Rev. B* **2011**, *84*, 224105.
[29] A. Pramanick, D. Damjanovic, J. E. Daniels, J. C. Nino, J. L. Jones, *J. Am. Ceram. Soc.* **2011**, *94*, 293.
[30] L. Chen, A. L. Roytburd, *Appl. Phys. Lett.* **2007**, *90*, 102903.
[31] N. Bassiri-Gharb, S. Trolier-McKinstry, D. Damjanovic, *J. Appl. Phys.* **2011**, *110*, 124104.